ELASTICITY, YIELDING AND EPISODICITY IN SIMPLE MODELS OF MANTLE CONVECTION

Running Title: Elasticity, Yielding and Episodicity

Hans-Bernd Muhlhaus

> ESSCC
> The University of Queensland
> St Lucia QLD 4072, Australia.
>
> CSIRO Division of Exploration and Mining
> 26 Dick Perry Ave
> Kensington WA 6051, Australia
>
> muhlhaus@esscc.uq.edu.au

Matt Davies

> ESSCC
> The University of Queensland
> St Lucia QLD 4072, Australia,
>
> matt@esscc.uq.edu.au

Louis Moresi

> School of Mathematical Sciences
> Building 28
> Monash University, VIC 3800, Australia
>
> louis.moresi@sci.monash.edu.au

ELASTICITY, YIELDING AND EPISODICITY IN SIMPLE MODELS OF MANTLE CONVECTION

Hans-Bernd Muhlhaus[1,2], Matt Davies[1] and Louis Moresi[3]

1   ESSCC, The University of Queensland, St Lucia QLD 4072, Australia, {muhlhaus,matt,gross}@esscc.uq.edu.au
2   CSIRO Division of Exploration and Mining, 26 Dick Perry Ave, Kensington WA 6051, Australia
3   School of Mathematical Sciences, Building 28, Monash University, VIC 3800, Australia, louis.moresi@sci.monash.edu.au

Abstract

We explore the implications of refinements in the mechanical description of planetary constituents on the convection modes predicted by finite element simulations. The refinements consist in the inclusion of incremental elasticity, plasticity (yield ing) and multiple simultaneous creep mechanisms in addition to the usual visco-plastic models employed in the context of unified plate-mantle models . The main emphasis of this paper rests on the constitutive and computational formulation of the model. We apply a consistent incremental formulation of the non-linear governing equations avoiding the computationally expensive iterations that are otherwise necessary to handle the onset of plastic yield. In connection with episodic convection simulations, we point out the strong dependency of the results on the choice of the initial temperature distribution. Our results also indicate that the inclusion of elasticity in the constitutive relationships lowers the mechanical energy associated with subduction events.

Introduction

The way a planet deforms in response to thermal or gravitational driving forces, depends on the material properties of its constituents. The Earth's behavior is unique in that its outermost layer consists of a small number of continuously moving plates. Venus, another planet of similar size and bulk composition to the Earth, displays signs of active volcanism but there is no evidence of plate movements or plate tectonics.

It is generally accepted that plate tectonics is a manifestation of mantle convection, a natural solid state convection process driven by the thermal gradients of a cooling planet with radiogenic heating. In this context, the pattern of surface motion is determined by the rheology of the cool thermal boundary layer. Purely viscous models of the lithosphere are not capable of producing the narrow plate boundary deformation zones and low strain-rate plate interiors which characterize plate tectonics. Research over the

past ten years in the area of computational unified plate-mantle models has demonstrated that additional model ingredients are required including temperature dependence of the viscosity combined with a finite material strength to enable the fracture processes necessary for plate formation (Moresi and Solomatov, 1998; Tackley, 1998). In square or cubic convection cells temperature dependence and a finite yield strength leads to three distinct modes of convection: If the yield strength is high compared to the thermal driving force, then convection is confined to a domain underlying a high viscosity, quasi rigid plate or lid. This mode of convection is usually designated stagnant lid convection. If the yield strength is low compared to the driving forces then yielding of the material at the cold boundary takes place and plate like regions form; this mode is designated mobile lid convection. In between the two extreme modes exists an episodic convection mode with alternating mobile and stagnant lid behavior.

In the following, we study the effect of physical and computational model refinements such as large strain elasticity, stress advection and an incremental decomposition (or tangent form) of the constitutive relationships. The model proposed here is an extension of the model proposed by Moresi et al (2002) in the context of a Lagrangian particle method. While the three distinct convection modes are clearly observed in square or cubic convection domains or in more general domains with periodic initial conditions, the sensitivity of the convection modes with respect to more general initial conditions is not clear and will be examined here as well. The paper is structured as follows: The model equations, constitutive relationships, and computational aspects are outlined in the following two sections. Simulation results are presented subsequently.

Model Formulation

The governing model equations consist of the stress equilibrium conditions

$$s'_{ij,j} - p_{,i} = r_0(1 - a_p(T - T_0))g_i \qquad (1)$$

and the heat equation

$$r_0 c_p(T_{,t} + v_j T_{,j}) = (kT_{,j})_{,j} + s'_{ij} D_{ij} + r_0 h \qquad (2)$$

Here we adopt the usual subscripted Cartesian tensor notation; postfixing subscripted differential indices after a comma and adopting the summation convention. In equation (1), s'_{ij} is the deviatoric stress, D_{ij} is the stretching, p is the pressure, $g_{i,}$ is parallel and opposite to the direction of gravity (i.e. such that $g = |g_i|$ is the gravitational constant) and a_p is the thermal expansion coefficient. In equation (2), r_0 is a reference density at the surface, c_p is the heat capacity, κ is the thermal conductivity and h is a specific energy source term (eg radiogenic heating). In the following examples we assume $h=0$ for simplicity.

In the formulation of the constitutive model we make the standard assumption that the stretching is the sum of an elastic and a visco- plastic part:

$$D_{ij} = D_{ij}^e + D_{ij}^{vp}. \qquad (3)$$

We assume incompressibility such that $D_{jj} = v_{j,j} = 0$, where v_j is the velocity. The visco-plastic stretching is then defined as $D_{ij}^{vp} = 1/2h_{eff} s'_{ij}$, where h_{eff} is the effective viscosity, and for the elastic part we assume

$$D_{ij}^e = \frac{1}{2m}(\dot{s}_{ij}^J)' \qquad (4)$$

where m is the elastic shear modulus and $\dot{s}_{ij}^J$ the Jaumann stress rate. The reader is referred to Kolymbas and Herle (2003) and Muhlhaus and Regenauer-Lieb (2004) for

recent discussions and comparisons between the various objective stress rates. The Jaumann stress rate is related to the material stress rate by

$$\dot{\boldsymbol{s}}_{ij}^{J} = \frac{\partial}{\partial t}\boldsymbol{s}_{ij} + v_k\boldsymbol{s}_{ij,k} - W_{ik}\boldsymbol{s}_{kj} + \boldsymbol{s}_{ik}W_{kj} \tag{5}$$

where W_{ij} is the non-symmetric part of the velocity gradient.

As a further refinement to this approach, the visco-plastic stretching is adopted in the form of a combined Newtonian and composite power law creep model (Muhlhaus and Regenauer-Lieb, 2004). The composite power law viscosity includes a contribution from both dislocation glide, with a typical power law exponent ($n \approx 3$), and plastic deformation, with temperature independent coefficients and a large exponent ($n_{pl} \approx 15$). The effective viscosity is then given by:

$$\boldsymbol{h}_{eff} = (\frac{1}{\boldsymbol{h}_N} + \frac{1}{\boldsymbol{h}_N(\frac{\boldsymbol{t}}{\boldsymbol{t}_0})^{1-n}} + \frac{1}{\boldsymbol{h}_Y(\frac{\boldsymbol{t}}{\boldsymbol{t}_Y})^{1-n_{pl}}})^{-1} \tag{6}$$

where $\boldsymbol{h}_Y$ is a reference viscosity for the plastic yield, τ_0 is the dislocation transition stress, τ_Y is the plastic yield stress and $\boldsymbol{t} = \sqrt{1/2\boldsymbol{s}'_{ij}\boldsymbol{s}'_{ij}}$ and $\boldsymbol{h}_N$ is the temperature-dependent Newtonian viscosity for which we adopt an Arrhenius relationship. This relationshit is of the form

$$\boldsymbol{h}_N = \boldsymbol{h}_{N0}\exp(AT_M/T) \tag{7}$$

where $\boldsymbol{h}_{N0}$ is a reference Newtonian viscosity, A is the activation energy and T_M is the melting temperature;

The yield stress, $\boldsymbol{t}_Y$, may depend on the accumulated visco-plastic strain, other state variables including damage variables (not considered here) and the pressure. For

completeness, although not used to obtain the results of this paper, we state an expression for the pressure dependence in the form

$$t_Y = t_{Y0} + bp \tag{8}$$

where b is the pressure sensitivity and t_{Y0} is the yield stress at zero pressure. Byerlee (1968) proposes a simplified criterion in which the pressure, p, of (8) is replaced by the overburden pressure rgz where z is the coordinate in the direction of gravity with $z=0$ on the cold boundary. The yield criterion (6) and Byerlee's simplified model are mathematically quite different however: The fourth order tensor relating the stress to the stretching is non-symmetric for the yield criterion (8), whereas the corresponding fourth order tensor is symmetric in the case of Byerlee's model. Non-symmetry is preferred (Rudnicki and Rice (1975), as non-symmetric models have a stronger tendency for strain localization.

The governing equations are highly non-linear with respect to the introduced constitutive relationships. In the numerical solution of the model equations the non-linearities are usually considered iteratively in that the effective viscosity (6) is updated in each step of the iteration on the basis of the results from the previous iteration step (e.g. Moresi and Solomatov, 1998). This approach is commonly referred to as a secant method. As an alternative, the convergence of this procedure can be improved drastically if the predictor step of the iteration is based on the incremental (=tangent) form of the constitutive relationship instead of the secant form as described above. In this paper we shall apply the tangent approach. The tangent or incremental form of the constitutive relations (3-8) have been derived in (Muhlhaus and Regenauer–Lieb, 2005) and are outlined here in the appendix for easy reference.

Computational Aspects

In the next section we present the results of finite element simulations of plane strain, natural convection problems in a rectangular L by H domain, where H is the dimension in the direction of gravity. Typical values are H=700km for upper mantle convection and H=3000km for whole mantle convection. We make the standard assumptions that the shear stress and normal velocity vanish on all boundaries of the domain; the temperatures are fixed on the top and the bottom and the normal gradient of the temperature vanish on the sides.

The non-dimensional forms of the governing equations are respectively given by

$$s'_{ij,j} - p^{th}_{,i} + Ra^c / gTg_i = 0 \tag{9}$$

$$T_{,t} + v_j T_{,j} = T_{,jj} + \frac{Di^c}{Ra^c} s'_{ij} D_{ij} \tag{10}$$

Equation (9) is obtained from equation (1) by decomposing the pressure as $p = r_0 g(H - x_z) + p^{th}$, where p^{th} is the pressure due to thermal expansion, x_z is the coordinate opposite to the direction of gravity and Ra^c and Di^c designate the computational Rayleigh number and the dissipation number respectively. The stresses in (9) and (10) are normalized with respect to $h^* t_D$ where h^* is a viscosity parameter and t_D is the characteristic thermal diffusion time. The significance of the viscosity parameter h^* follows from the transformation (for numerical purposes) of the Arrhenius law (see below). The thermal diffusion time, t_D, is given by the expression

$$t_D = \frac{r_0 c_p H^2}{k} \tag{11}$$

With $k/(r_0 c_p) = 10^{-6} m^2 s^{-1}$ we obtain $10^{17} < t_D < 10^{19} s$. The Ra^c and Di^c, consistent with the way the stresses are non-dimensionalised, are defined as

$$Ra^c = \frac{r_0^2 c_p g \boldsymbol{a} \Delta T H^3}{kh*} \quad \text{and} \quad Di^c = \frac{\boldsymbol{a} r_0 g H}{r_0 c_p} \tag{12}$$

In (12) ΔT is the temperature difference between the hot and the cold boundary of the domain under consideration. In the present paper we assume $Di^c=0$ since our main focus here is on the influence of temperature dependence of the viscosity, plasticity and elasticity. The temperature and the velocities are non-dimensionalised with respect to $\boldsymbol{D}T$ and H/t_D respectively.

The governing equations have been implemented using the computational software toolkit *Escript* (Davies et al, 2004). Through adoption of the *Python* scripting language, *Escript* is designed to provide an extensible interface to various computational kernel modules such as equation solvers and matrix assembly routines. These kernels in turn provide implicit parallelism, permitting an expert user to focus on scripting the computational scheme for a model as opposed to the low-level implementation detail of parallelization primitives. In this way it is possible to script high performance parallel software without scripting a single line of parallel code. All of the parallelism is delegated to (and encapsulated within) the computational kernel modules selected for the task at hand.

An important computational kernel module interfaced to *Escript* is the *Finley* FEM library (Davies et al, 2004). To use *Finley*, an unsteady initial boundary value problem (IBVP) must first be transformed into a sequence of steady BVPs by means of a suitable time discretisation procedure applied at each time step. The steady, linear BVP can then be provided to *Finley* which will then assemble a stiffness matrix associated with a given unstructured mesh using a discretisation based on the standard variational

formulation. For an unknown function u, the system of partial differential equations (PDEs) associated with a BVP can be defined through the specification of the coefficients of the following templated system:

$$-\left(A_{ijkl}u_{k,l}\right)_{,j} - \left(B_{ijk}u_{k}\right)_{,j} + C_{ikl}u_{k,l} + D_{ik}u_{k} = -X_{ij,j} + Y_{i}, \quad x_{i} \in G_{i} \tag{13}$$

The tensorial coefficients A, B, C, D, X, and Y are functions of their location in the physical domain. In a similar manner, *Finley* also accepts a system of implicit natural and Dirichlet boundary conditions for which template parameters can be specified.

In the implementation we solve sequentially the stress equilibrium equation and the heat equation. The incompressibility constraint is satisfied iteratively by means of the algorithm

$$p^{a+1} = p^{a} - \mathbf{l}\, v_{j,j}^{a+1} , \; \alpha=1,2,3,\dots \tag{14}$$

where α is the iteration counter $\mathbf{l} = \mathbf{l}_{0}\mathbf{m}_{\mathit{eff}}\,dt$ is a penalty function (see appendix for definition of the effective shear modulus μ_{eff}). A typical value for the constant $\mathbf{l}_{0}$ is 100. In connection with direct solvers, convergence is fastest with a larger value for $\mathbf{l}_{0}$. However, there are usually limits to the value of $\mathbf{l}_{0}$ in connection with iterative solvers. After the pressure iteration the stresses are calculated by solution of matrix problems for each column of the stress tensor. For consistency the order of interpolation is one order less than the one for the velocities. For the velocities and the temperature we use eight noded rectangular elements with bi-quadratic shape functions. For the stresses we use bilinear rectangular elements and evaluate the values of the stresses at the mid side

nodes after the solution of the stress equations. Subsequently the heat equation is solved using backward Euler time differencing.

The stress equations and the heat equation involve convective derivatives of the stresses and temperature respectively. We use a basic upwinding scheme [(Zienkiewicz and Taylor and Zienkiewicz, 2000, p. 30]) to avoid spurious oscillations of the fields in advection dominated regimes. The common procedure to implement the standard streamline upwind Petrov-Galerkin (SUPG) formulation is to modify the test or weight functions used in the formulation of the finite element method. However, in the present case, it is convenient to modify the differential equation. In our formulation we replace the material time derivative of a function a as follows:

$$a_{,t} + v_j a_{,j} \leftarrow a_{,t} + v_j a_{,j} - ((a_{,t} + v_j a_{,j}) \frac{h}{2\sqrt{v_k v_k}} v_i)_{,i} \tag{15}$$

The function a can be either a scalar (e.g. temperature), a vector (e.g. velocity) or a tensor (e.g. stress). For pure advection problems, this approach is equivalent to the SUPG method.

For unstructured meshes, the (mid) time step dt^+ is determined from a 1st order implicit extrapolation of the Courant condition $dt = C \frac{h}{v_{max}}$ where C is an appropriate Courant number, h is the discretization scale and and $v_{max}(t) \in \mathbf{C}^1$ is the maximum magnitude of the nodal point velocities. For the results of this paper the following condition is used:

$$dt^+ = \frac{2Ch}{v_{max}^{(t+dt)} + v_{max}^{(t)}} = \frac{\sqrt{dt^-(dt^- v_{max}^{(t)\,2} + 2(v_{max}^{(t)} - v_{max}^{(t-dt)})Ch)} - dt^- v_{max}^{(t)}}{v_{max}^{(t)} - v_{max}^{(t-dt)}} \tag{16}$$

Due to the adaptive nature of the 1st order implicit extrapolation scheme, larger values of C can be trialled in a guarded manner, potentially yielding larger time steps.

In the case of an explicit algorithm, C is set to ½ for stability of the numerical solution in connection with regular grids. As a fully implicit integration scheme is used, the Courant (-like) condition is not needed for numerical stability. However, we retain the condition to achieve accuracy of the transient solution of the non-linear equations. In general, higher order approaches such as the condition (16) can be used if v_{max} can be shown to be continuously differentiable to the required order. Furthermore, a corresponding initial predictor of the velocity field for the next time-step can then be calculated if required and may in turn be used as a time step corrector.

In the convection study in the next section we ignore the pressure dependence of T_M in the Arrhenius relation. The main emphasis in the study will be on the role of elasticity, power law creep and plasticity on the emergence of different modes of convection. In the dimensionless formulation we write the Arrhenius relationship as follows (see Tackley, 1998):

$$\boldsymbol{h}_{N0}\exp(AT_M/T) \rightarrow \boldsymbol{h}_{N0}\exp(\frac{2\hat{A}}{3})\exp(\hat{A}(\frac{1}{1+T}-\frac{2}{3})) = \boldsymbol{h}*\exp(\hat{A}(\frac{1}{1+T}-\frac{2}{3})) \qquad (17)$$

The exponent of (15) varies between 0 for T=0.5, and $-\hat{A}/6$ or $\hat{A}/3$, for T=1.0 or T=0.0 respectively. For $\hat{A}=23$, this corresponds to a Newtonian viscosity contrast of about 10^5 across the convection cell. In the absence of convection, the Newtonian viscosity varies slowly due to temperature change in the lower half of the cell, from 1 in the middle to 0.022 on the bottom and rapidly in the upper half from 1.0 to 2087.0 on the top.

Simulations

In the first subsection we consider the effect of refinements such as elasticity and stress advection for the case of episodic convection. Episodic convection is suited for this study as it involves phases of rapid change of the flow pattern within which we expect elasticity to be important and stagnant lid phases where elasticity is expected to be unimportant. In the second subsection we consider the influence of non-periodic initial conditions in connection with two dimensional 4 by 1 convection cells on the persistence of the different convection modes.

The temperature dependence of the viscosity was given by (17) with $\hat{A} = 23$ which gives a viscosity ratio from the cold to the hot boundary due to temperature alone of 10^5. More extreme viscosity contrasts can easily be considered in the present formulation because the upper limit for the effective dimensionless viscosity is set by the dimensionless elastic shear modulus and the time increment $(\boldsymbol{m}t_D / \boldsymbol{h}^*)\boldsymbol{d}t$. We assign $Ra^c = 10^4$, $\tau_0 = 0.866 \ 10^{2.5}$, $\tau_Y = 3\tau_0$ (i.e. a constant for ideal plasticity) and $(\boldsymbol{m}/\boldsymbol{h}^*)t_D = 10^4$. In the simulations we used the power law plasticity model with $n_Y = 15$ and $\eta_Y = \eta_{N0}$ (see also the appendix for further detail). The initial temperature distribution was

$$T = \frac{1}{10}\sin(x_2\boldsymbol{p})\cos(x_1\boldsymbol{p}) + (1 - x_2) \tag{18}$$

The corresponding Nusselt number *vs*. time plot is shown in Figure 1. After initial, rapidly decaying, primarily elastic oscillations (not shown), the system settles temporarily into a stagnant lid mode of convection similar to the temperature and velocity profile shown in Figure 2a. During this initial period, stress accumulates until the yield stress is reached within the cold boundary layer. The locally-increased mobility was accompanied by thermal advection, a narrow plume formed, hot material was advected underneath toward a narrow, cold boundary layer. This process continued

until the cold layer plunged back into the lower mantle along the boundary opposite to the plume (Figure 2b). This process repeated itself at approximately regular intervals. The initial time intervals between the first peaks of the episodic mode in Figure 1 are 0.071, 0.044, 0.045, 0.044, with constant intervals afterward. Also shown in Figure 1 are the Nusselt numbers for mobile lid convection (obtained for $\tau_Y = \tau_0$) and stagnant lid convection ($t_Y \geq 6t_0$).

Figure 1

The length y of the vertical lines plotted along the cold (top) boundary of the velocity plots in Figures 2, 3 and 6 are given by:

$$y = \frac{\max|v_1| - |v_1|_{x_2=1}}{\max|v_1|} \tag{19}$$

where $\max|v_1|$ is the magnitude of the largest horizontal velocity anywhere in the convection cell and $|v_1|_{x_2=1}$ is the local horizontal velocity on the top boundary surface. Within the framework of our model, $|v_1|_{x_2=1}$ is representative of the plate velocity. If $y = 0$ at a point on the boundary, then this point is mobile with a velocity of $\max|v_1|$. A comparison the mobile lid convection mode (Figure 3) with the stagnant lid phase of the episodic convection mode (Figure 2a) indicates that the horizontal velocities on the cold boundary are largest for the mobile lid convection mode. Large segments of the top layer with values of y close to zero as in Figure 3 or during episodic convection in Figure 2b are indicative of plate like behaviour.

Figure 2a

Figure 2b

The isotherms and velocity arrows displayed on Figures 2a and 2b are representative for the stagnant lid phases (minima of Nusselt plots in Figure1) and the subduction events (maxima of Nusselt plots) for an episodic convection mode. The isotherms and velocity arrows corresponding to the steady state of mobile lid convection is shown in Figure 3.

Figure 3

Next we investigate the influence of the choice of the initial temperature distribution. Will the three distinct modes of convection be stable with respect to a change of the initial conditions? We adopt a nonharmonic condition at t=0 such that

$$T = \frac{1}{10} \sin(x_2 \boldsymbol{p}) \cos(x_1^2 \boldsymbol{p} / L) + (1 - x_2) \tag{20}$$

Figure 4 shows Nusselt number *vs*. time plots corresponding to the three cases considered before. The mobile lid mode settles at a slightly lower Nusselt number at steady state but the features of the isotherms and velocity arrows are qualitatively the same as for the case with harmonic initial conditions. Instead of the expected episodic convection mode we observed for harmonic initial conditions, we observe a tendency toward mobile lid convection, although the initial oscillation decays at a slower rate than for the mobile lid mode with $\boldsymbol{t}_Y = \boldsymbol{t}_0$. For non-harmonic initial conditions, the stagnant lid mode of Figure 5 becomes comparable to a dampened episodic convection

mode. In this case, we observe an extended oscillatory phase but again ultimately the system settles into a steady state (observable in Figures 4 and 5).

Figure 4

Figure 5

A comparison of the distribution and length of vertical lines (see equation (19)) on top of the velocity plots of Figures 5 and 6, indicates that in contrast to the mobile lid convection mode, the horizontal velocities on the cold boundary are much smaller than the horizontal velocities closer to the hot boundary..

Figure 6

The influence of the elastic shear modulus becomes important if $(\mu/\eta*)t_D < 10^5$. A comparion of the results reveals that there is little difference between the $(\mu/\eta*)t_D = 10^5$ and the $(\mu/\eta*)t_D = 10^{20}$ cases. Smaller shear moduli cause a shortening of the period between the subduction events.

Figure 7

By multiplying (9) with v_i, integration of the resulting expression over the domain V and application of Gauss theorem we obtain the total mechanical power, $\dot{W}$, as

$\dot{W} = RaV(Nu - 1)$. The reader is referred to Parmentier et al (1976) for details of the derivation. This equation relates the area under the graph of a Nusselt plot to the mechanical work associated with the convection process. In particular, the area under a spike of the Nusselt plot is proportional to the work associated with a subduction event. This area decreases with the decreasing value of the elastic shear modulus. It is remarkable that this effect is evident in a global energy measure such as the Nusselt number.

Conclusions

We have outlined a formulation for visco-elastic convection based on a combined Newtonian and composite power law rheology where the effect of plastic yielding is considered as a power law term with a high ($n_{pl} \approx 15$) power law coefficient (6). The model is suitable for studying the geodynamics of mantle convection amongst other problems in geophysical flow. The nonlinear equations of motion are solved incrementally based on a consistent tangent formulation producing second order accurate results and avoiding the computationally expensive iterations that are otherwise necessary to handle the onset of plastic yield in most cases. In Moresi and Solomatov (1998) and Tackley (1998), plastic yielding is considered by introducing an upper limit to the viscosity given by the ratio of the yield stress and the equivalent viscous strain rate. Since the strain rate at the current time is unknown, an initial estimate has to be based on the strain rate from the last time step producing a result of first order accuracy. For this reason, a time consuming, iterative approach is necessary. The iterative approach is often more time consuming than the present incremental approach including the occasional iterative reduction of residuals. With the iterative approach, the

constitutive operator is sparser than in the consistent incremental approach, which can be used to advantage.

The convection model with a strongly temperature dependent viscosity has some unique characteristics: the produced strains can be very large, necessitating a fluid-dynamics formulation, yet the relaxation time in the cool thermal boundary layer is significant compared to the characteristic time associated with fluid flow. In the bulk of the fluid, the relaxation time is small compared to the time taken for convective features to evolve due to the much lower viscosity of the warm fluid.

As elastic stresses in the strongly convecting part of the system relax rapidly, the introduction of elasticity does not produce a qualitative change to the stagnant lid convection regime (see Solomatov, 1995). In the episodic and mobile lid modes, there is competition between the build-up of stresses in the cool lid and the stress-limiting effect of the yield criterion. Our results show that the introduction of elastic deformation does not quantitatively influence this balance either, although we do expect a difference in the distribution of stresses in the lid, which explains the variation in the onset of overturns and their increasing frequency which we observed as the elastic shear modulus was reduced. It should be noted that a global flow characteristic such as the Nusselt number may not be suitable to investigate the effect of elasticity. This is because the significant elastic effect is limited to the plate (or top boundary layer) which occupies only a small fraction of the total volume of the convection cell. In a future study we plan to differentiate between the energy rates associated with elastic, Newtonian creep, power law creep and plastic deformation, evaluated in those parts of the convection cell in which plate like behavior is expected (e.g. for $T < 1400K$, see Schubert et al 2001, p.26).

The presence of an elastic deformation mechanism also permits significant deformation of the highly viscous lid with lower energy rates as the plate is able to bend without

necessarily having to form a plastic hinge. This is reflected in lower energy levels during episodic overturns which we observed by integrating the system Nusselt number. In the Earth, this effect may be important in subduction zones where the prediction of dissipation rates due to slab bending is larger than what seems physically plausible in this context (Conrad and Hager, 1999).

We observed a breakdown in the highly regular boundary layer turnover time when transitioning from harmonic initial condition to a non-harmonic initial condition.

This is similar to the results of Moresi and Solomatov (1998), who noted for the purely viscous case that the regularity of the episodic mode was an artifact of the small convection domains. Once we break the perfect symmetry of the convection pattern, the evolution also becomes significantly more time-dependent.

References

Byerlee, J. (1965), The brittle ductile transition in rocks, J. Geophys. Res., 73, 4741-4750.

Conrad, C.P. and Hager, B.H. (1999). Effects of plate bending and fault strength at subduction zones on plate dynamics. J. Geophys. Res., 104 (B8), 17551-17571.

Davies, M., Gross, L. and Muhlhaus, H.-B. (2004), Scripting high performance earth systems simulations on the SGI Altix 3700, Proc. 7th Int. Conf. HPC Grid Asia Pac. Reg., 244-251.

Kolymbas, D. and Herle, I. (2003), Shear and objective stress rates in hypoplasticity, Int. J. Numer. Anal. Meth. Geomech., 27, 733-744.

Moresi, L., Dufour, F. and Muhlhaus, H.-B. (2002), Mantle convection models with viscoelastic/brittle lithosphere: Numerical methodology and plate tectonic modeling, Pure Appl. Geophys., 159 (10), 2335.

Moresi, L., and Solomatov, V.S. (1998), Mantle convection with a brittle lithosphere: thoughts on the global tectonic styles of the Earth and Venus, Geophys. J. Int., 133 (6), 669-682.

Muhlhaus, H.-B. and Regenauer-Lieb, K. (2004), A Self Consistent Plate Mantle Model that Includes Elasticity: Computational Aspects and Application to Basic Modes of Convection, Geophys. J. Int., submitted May 2004.

Parmentier, E.M., Turcotte, D.L. and Torrance, K.E. (1976), Studies of finite amplitude non-Newtonian thermal convection with application to convection in the Earth mantle, J. Geophys. Res., 81,1839-1846.

Rudnicki, J.W. and Rice, J.R. (1975), Conditions for the localisation of deformation in pressure-sensitive dilatant materials, J. Mech. Phys. Sol., 23, 371-394.

Schubert,G., Turcotte, D.L. and Olson, P., Mantle Convection in the Earth and Planets (Cambridge University Press, Cambridge 2001).

Tackley, P. (1998), Self-consistent generation of tectonic plates in three-dimensional mantle convection, Earth and Planetary Science Letters, 157, 9-22.

Solomatov, V.S. (1995), Scaling of temperature- and stress- dependent viscosity convection, Phys. Fluids, 7, 266-274.

Zienkiewicz, O.C. and Taylor R.L., The Finite Element Method, Vol. 3, 5th Ed., (Butterworth/Heinemann 2000).

Appendix

The constitutive relation (3) can be rewritten as:

$$D_{ij} = \frac{1}{2\boldsymbol{m}}\dot{\boldsymbol{s}}_{ij}^{\prime J} + (\frac{1}{2\boldsymbol{h}_N} + \frac{1}{2\boldsymbol{h}_N(\frac{\boldsymbol{t}}{\boldsymbol{t}_0})^{1-n}})\boldsymbol{s}_{ij}^{\prime} + \dot{\boldsymbol{g}}^p\frac{\boldsymbol{s}_{ij}^{\prime}}{2\boldsymbol{t}} \qquad \text{A1}$$

Where we have adopted a power law expression for the equivalent plastic strain rate, $\dot{\boldsymbol{g}}^p$, of the form:

$$\dot{\boldsymbol{g}}^p = \frac{\boldsymbol{t}_Y}{\boldsymbol{h}_Y}(\frac{\boldsymbol{t}}{\boldsymbol{t}_Y})^{n_{pl}} \qquad \text{A2}$$

The coefficient of $\boldsymbol{s}_{ij}^{\prime}/2$ in (A1) obtained by inserting (A2) into (A1) is equal to the inverse of the effective viscosity (6). The incremental form of our constitutive relationship is optained by inserting the expansions $\boldsymbol{s}_{ij}^{t+dt} = \boldsymbol{s}_{ij}^{t} + \boldsymbol{ds}_{ij}$, $T^{t+dt} = T^t + \boldsymbol{dT}$, $p^{t+dt} = p^t + \boldsymbol{dp}$ into (A1). Retaining only the linear terms in the stress, temperature and pressure increments yields:

$$D_{ij} - \frac{\boldsymbol{dt}}{2\boldsymbol{h}_{eff}}(W_{ik}\boldsymbol{s}_{kj} - \boldsymbol{s}_{ik}W) - \frac{1}{2\boldsymbol{m}}\boldsymbol{s}_{ij,k}^{\prime}v_k = \frac{1}{2\boldsymbol{m}_{eff}\boldsymbol{dt}}\boldsymbol{ds}_{ij}^{\prime J} + (\underbrace{\frac{1}{h_{vis}} + \frac{1}{h_Y}}_{1/h})\frac{\boldsymbol{s}_{ij}^{\prime}}{2\boldsymbol{t}}\frac{\boldsymbol{s}_{kl}^{\prime}}{2\boldsymbol{t}}\boldsymbol{ds}_{kl}^{\prime J} +$$
$$+ \frac{1}{2\boldsymbol{h}_{eff}}\boldsymbol{s}_{ij}^{\prime} + \frac{1}{2\boldsymbol{h}_{eff}}\boldsymbol{s}_{ij}^{\prime}(\frac{\boldsymbol{dT}}{h_T} + \frac{\boldsymbol{dp}}{h_p}) \qquad \text{A3}$$

where:

$$\dot{\boldsymbol{s}}_{ij}^{\prime} = \boldsymbol{s}_{ij,t}^{\prime} + \boldsymbol{s}_{ij,k}^{\prime}v_k \qquad \text{A4}$$

$$\boldsymbol{ds}_{ij}^{J} = (\boldsymbol{s}_{ij,t} - W_{ik}\boldsymbol{s}_{kj} + \boldsymbol{s}_{ik}W)\boldsymbol{dt}, \quad \boldsymbol{dT} = T_{,t}dt, \quad \boldsymbol{dp} = p_{,t}dt \qquad \text{A5}$$

$$h_{vis} = \frac{1}{(n-1)} \boldsymbol{h}_N \left(\frac{\boldsymbol{t}}{\boldsymbol{t}_0}\right)^{1-n}, \quad h_Y = \frac{1}{(n_{pl}-1)} \boldsymbol{h}_Y \left(\frac{\boldsymbol{t}}{\boldsymbol{t}_Y}\right)^{1-n_{pl}} \qquad \text{A6}$$

$$h_T = \frac{T^2}{AT_M}, \quad h_p = -\frac{T}{A\frac{\partial T_M}{\partial p}}, \qquad \text{A7}$$

$$\boldsymbol{m}_{eff} = \left(\frac{1}{\boldsymbol{m}} + \frac{\boldsymbol{dt}}{\boldsymbol{h}_{eff}}\right)^{-1}. \qquad \text{A8}$$

Here, $\boldsymbol{h}_{eff}$ and $\boldsymbol{h}_N$ are defined by (6) and (7) respectively. Inversion of A3 yields:

$$\boldsymbol{ds}_{ij}^{\prime J} = (\boldsymbol{m}_{eff}\boldsymbol{dt}(\boldsymbol{d}_{ik}\boldsymbol{d}_{jl} + \boldsymbol{d}_{jk}\boldsymbol{d}_{il}) - \frac{(\boldsymbol{m}_{eff}\boldsymbol{dt})^2}{h + \boldsymbol{m}_{eff}\boldsymbol{dt}} \frac{\boldsymbol{s}_{ij}^{\prime}}{\boldsymbol{t}} \frac{\boldsymbol{s}_{kl}^{\prime}}{\boldsymbol{t}})(D_{kl} - \frac{\boldsymbol{s}_{kl,m}^{\prime}v_m}{2\boldsymbol{m}}) -$$

$$\frac{\boldsymbol{m}_{eff}\boldsymbol{dt}}{\boldsymbol{h}_{eff}} (1 - \frac{\boldsymbol{m}_{eff}\boldsymbol{dt}}{h + \boldsymbol{m}_{eff}\boldsymbol{dt}})(1 + \frac{\boldsymbol{dT}}{h_T} + \frac{\boldsymbol{dp}}{h_p})\boldsymbol{s}_{ij}^{\prime} - \frac{\boldsymbol{m}_{eff}\boldsymbol{dt}^2}{\boldsymbol{h}_{eff}}(W_{ik}\boldsymbol{s}_{kj} - \boldsymbol{s}_{ik}W) \qquad , \qquad \text{A9}$$

where $h = \frac{h_{vis}h_Y}{h_{vis} + h_Y}. \qquad \text{A10}$

The function h_p in (A3) and (A9) considers the pressure dependence of T_M. The slope of the $T_M - p$ curve is usually assumed as constant; a typical order of magnitude value for the slope is 10^{-7} K Pa^{-1}. For n=1 and $\boldsymbol{m} \to \infty$ we obtain Newtonian flow with the viscosity ½ η_N .

In many practical applications the velocity-pressure incompressibility and the heat equation are solved and advanced sequentially. In this case, the terms associated with $\boldsymbol{dT}$ and $\boldsymbol{dp}$ in equation (A9) are not needed. In linear instability analyses, however, the full incremental form (A9) is required.

In the viscous limit, $\boldsymbol{m} \to \infty$, (A9) reduces to:

$$\boldsymbol{ds}_{ij}^{\prime} = (\boldsymbol{h}_{eff}(\boldsymbol{d}_{ik}\boldsymbol{d}_{jl} + \boldsymbol{d}_{jk}\boldsymbol{d}_{il}) - \frac{\boldsymbol{h}_{eff}^2}{h + \boldsymbol{h}_{eff}} \frac{\boldsymbol{s}_{ij}^{\prime}}{\boldsymbol{t}} \frac{\boldsymbol{s}_{kl}^{\prime}}{\boldsymbol{t}})D_{kl} - (1 - \frac{\boldsymbol{h}_{eff}}{h + \boldsymbol{h}_{eff}})(1 + \frac{\boldsymbol{dT}}{h_T} + \frac{\boldsymbol{dp}}{h_p})\boldsymbol{s}_{ij}^{\prime} \qquad \text{A11}$$

In steady states, the stress, temperature and pressure increments vanish so that the remaining terms in (A11) cancel. This cancellation is indeed the case as can be shown by insertion of $D_{ij} = 1/2\boldsymbol{h}\boldsymbol{s}'_{ij}$.

The limit $\boldsymbol{h}_N \to \infty$ does not yield a simpler expression for the incremental relationship (A9) since the effective moduli still depend on the viscosity $\boldsymbol{h}_Y(\boldsymbol{t}_Y/\boldsymbol{t})^{n_{pl}-1}$. However, in the rate independent limit as $n_{pl} \to \infty$, this viscosity tends to infinity so that the expression A14 reduces to

$$\partial \boldsymbol{s}'_{ij}/\partial t = (\boldsymbol{m}(\boldsymbol{d}_{ik}\boldsymbol{d}_{jl} + \boldsymbol{d}_{jk}\boldsymbol{d}_{il}) - \boldsymbol{m}\frac{\boldsymbol{s}'_{ij}}{\boldsymbol{t}}\frac{\boldsymbol{s}'_{kl}}{\boldsymbol{t}})(D_{kl} - \frac{1}{2\boldsymbol{m}}\boldsymbol{s}'_{ij,k}v_k) + (W_{ik}\boldsymbol{s}_{kj} - \boldsymbol{s}_{ik}W_{kj}) \qquad \text{A12}$$

In the above derivation it was assumed that the yield stress is constant. A large deformation model with power law plasticity and state variable dependence of the yield stress will be presented in a forthcoming paper.

Figure Captions

Figure 1. A comparison of Nusselt numbers for stagnant-lid (lowest at steady state), episodic and mobile lid convection modes arising from harmonic initial conditions (18). The plastic yield stress, τ_Y, is 1,3, or 6 times the Newtonian-power law transition stress $\tau_0 = 0.866\ 10^{2.5}$. An Arrhenius relation describes the temperature dependence of creep with viscosity contrast across the layer of 10^5. The composite power law exponents are $n=3$ and $n_{pl}=15$ for dislocation glide and plastic deformation respectively. The dimensionless shear modulus is $\mu = 10^4$.

Figure 2a. Typical temperature and velocity distributions for an episodic convection mode at a minimum of the Nusselt number (refer to Figure 1). The length of the vertical lines on top of the velocity plot are inversely proportional to the cold boundary velocities.

Figure 2b. Typical temperature and velocity distributions for an episodic convection mode at a maximum of the Nusselt number (refer to Figure 1). The length of the vertical lines on top of the velocity plot are inversely proportional to the cold boundary velocities.

Figure 3. Typical temperature and velocity distributions at steady state for the mobile lid convection mode. The length of the vertical lines on top of the velocity plot are inversely proportional to the cold boundary velocities. For mobile lid convection, significant parts of the top layer move like rigid bodies.

Figure 4 A comparison of Nusselt numbers for convection modes arising from nonharmonic initial conditions (20). The parameters are the same as those described in Figure 1.

Figure 5 A comparison between Nusselt numbers for stagnant lid convection arising from a harmonic initial temperature distribution (18) and a nonharmonic initial temperature distribution (20).

Figure 6. Temperature and velocity distributions at steady state for the stagnant lid convection mode arising from a nonharmonic initial temperature distribution (20). The length of the vertical lines on top of the velocity plot are inversely proportional to the cold boundary velocities. Here the horizontal velocities on top are only a small fraction of the horizontal velocities closer to the hot boundary (compare with Figure3).

Figure 7. Influence of the elastic shear modulus: $(\mu/\eta*)t_D = 0.25 \times 10^4$, 0.5×10^4, 10^5, 10^{20}; $n=3$, $n_{pl}=15$, $Ra^c=10^4$, $\tau_0=0.866 \ 10^{2.5}$, $\tau_Y=3\tau_0$.
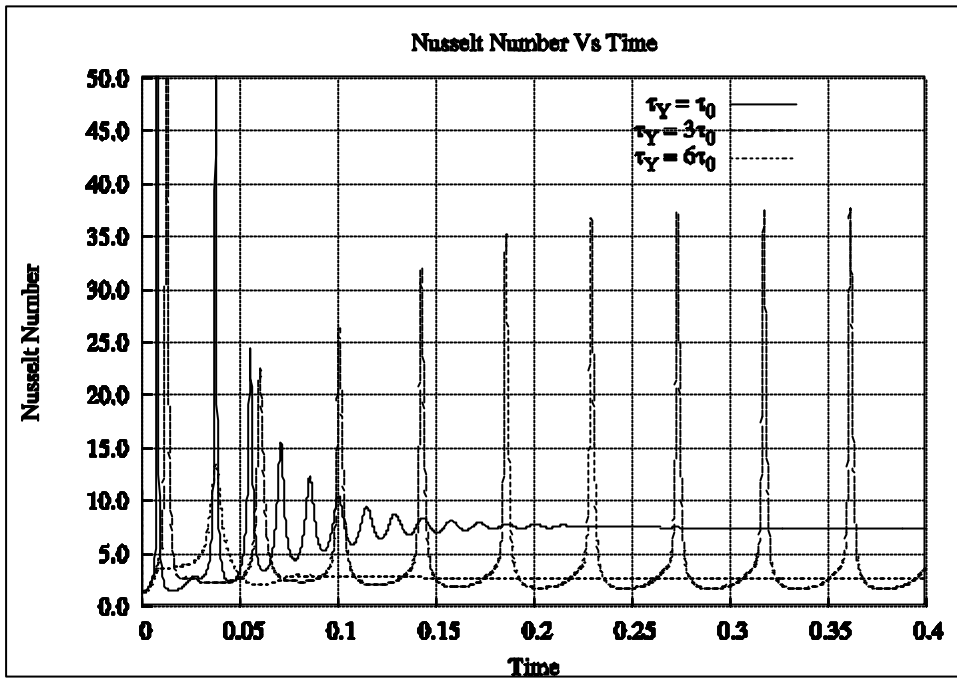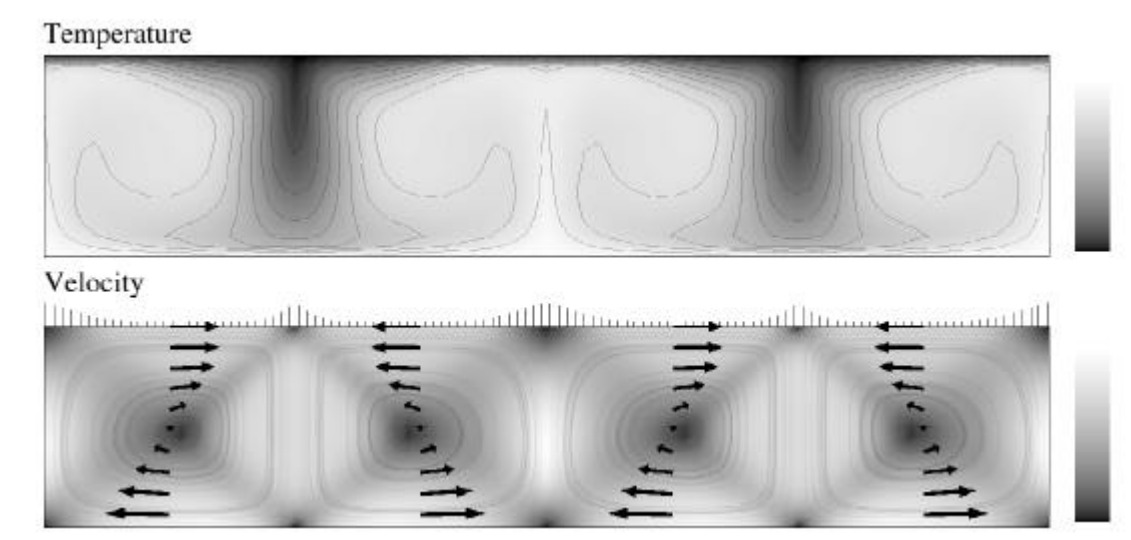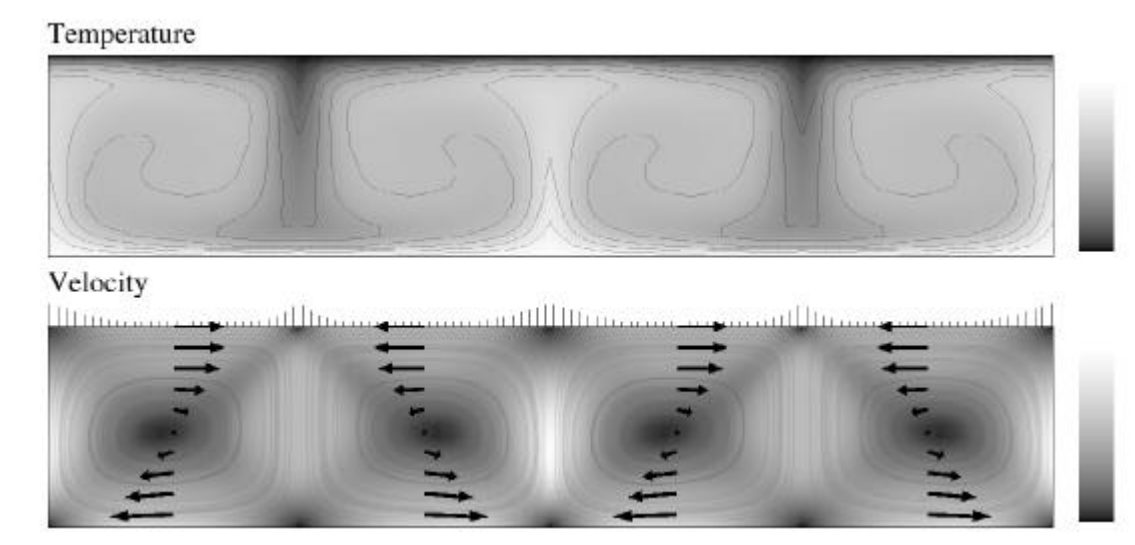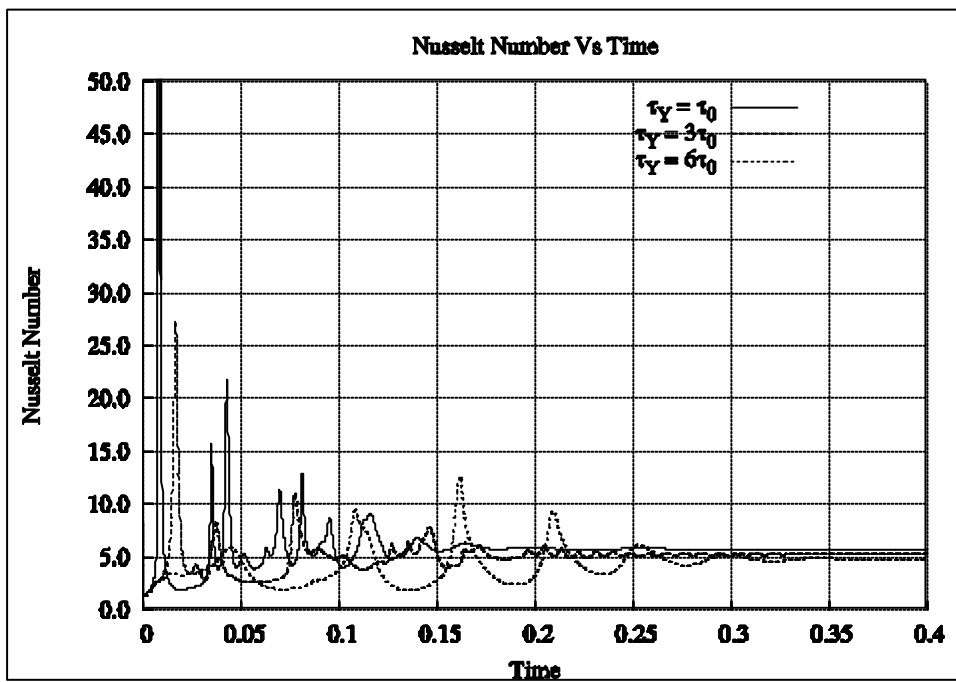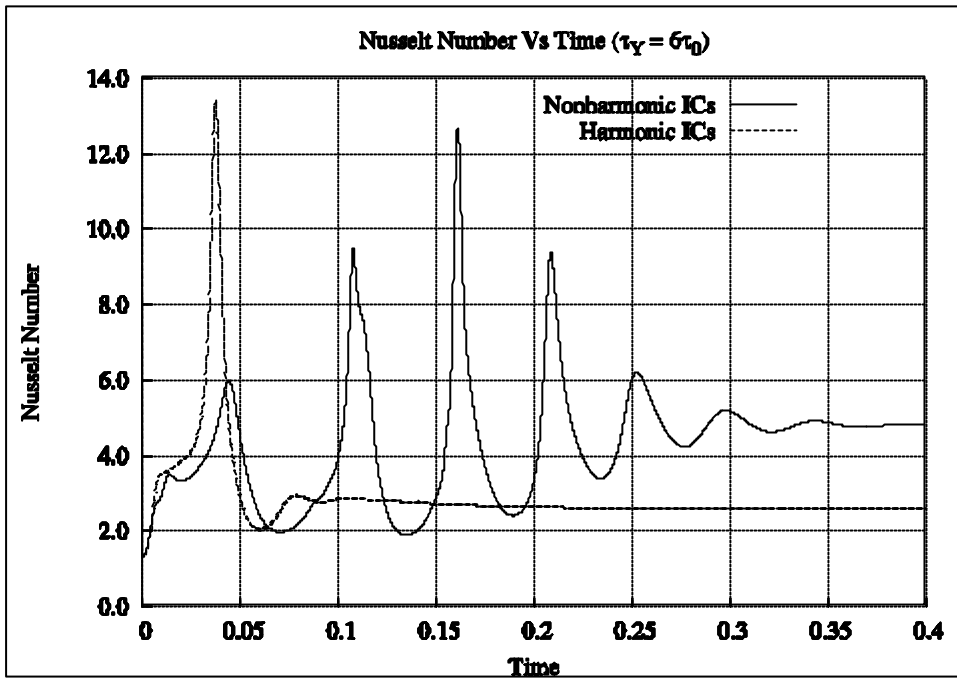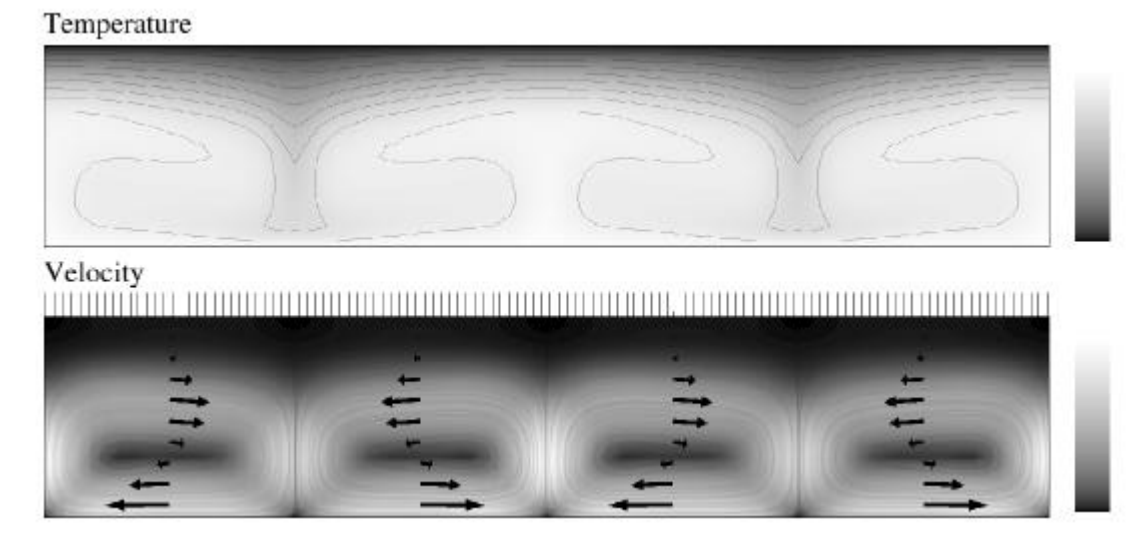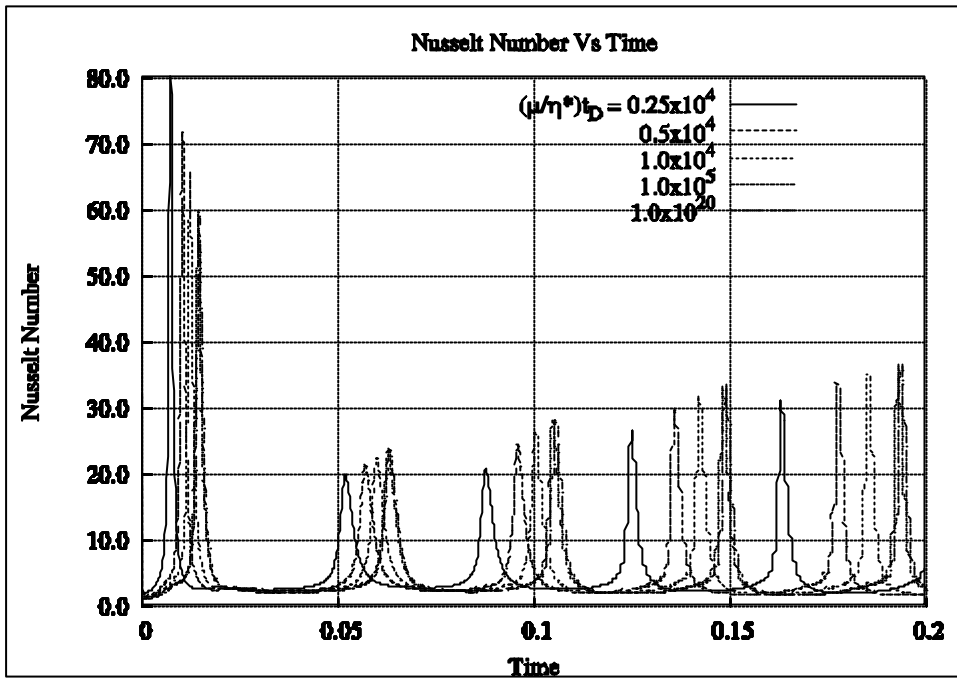
Figure 1.
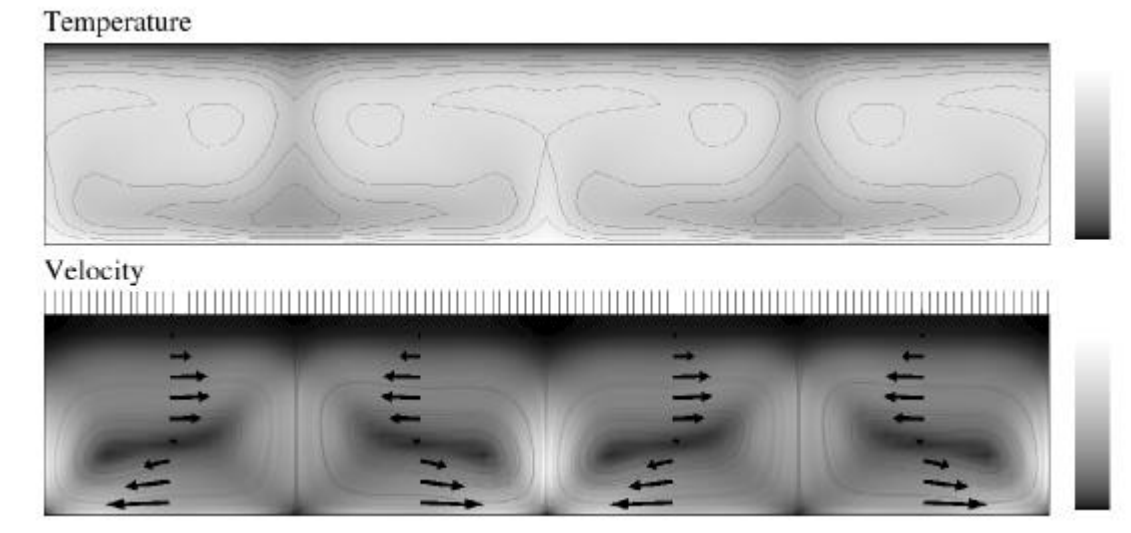
Figure 2a.

Figure 2b.

Figure 3.

Figure 4.

Figure 5.

Figure 6.

Figure 7.